Biomaterials 84 (2016) 1–12

Contents lists available at ScienceDirect

Biomaterials

journal homepage: www.elsevier.com/locate/biomaterials

Inhibition of tumor growth and metastasis by photoimmunotherapy targeting tumor-associated macrophage in a sorafenib-resistant tumor model

Chenran Zhang [a], Liquan Gao [a], Yuehong Cai [b], Hao Liu [a], Duo Gao [a], Jianhao Lai [a], Bing Jia [a], Fan Wang [a, c], Zhaofei Liu [a, *]

[a] Medical Isotopes Research Center and Department of Radiation Medicine, School of Basic Medical Sciences, Peking University Health Science Center, Beijing 100191, China
[b] Division of Medical Sciences, Weifang People's Hospital, Weifang 261000, China
[c] Interdisciplinary Laboratory, Institute of Biophysics, Chinese Academy of Sciences, Beijing 100101, China

ARTICLE INFO

Article history:
Received 28 November 2015
Received in revised form
11 January 2016
Accepted 12 January 2016
Available online 13 January 2016

Keywords:
Tumor-associated macrophage (TAM)
Tumor microenvironment
Molecular imaging
Photoimmunotherapy
Tumor metastasis

ABSTRACT

Tumor-associated macrophages (TAMs) play essential roles in tumor invasion and metastasis, and contribute to drug resistance. Clinical evidence suggests that TAM levels are correlated with local tumor relapse, distant metastasis, and poor prognosis in patients. In this study, we synthesized a TAM-targeted probe (IRD-αCD206) by conjugating a monoclonal anti-CD206 antibody with a near-infrared phthalocyanine dye. We then investigated the potential application of the IRD-αCD206 probe to near-infrared fluorescence (NIRF) imaging and photoimmunotherapy (PIT) of tumors resistant to treatment with the kinase inhibitor sorafenib. Sorafenib treatment had no effect on tumor growth in a 4T1 mouse model of breast cancer, but induced M2 macrophage polarization in tumors. M2 macrophage recruitment by sorafenib-treated 4T1 tumors was noninvasively visualized by in vivo NIRF imaging of IRD-αCD206. Small-animal single-photon emission computed tomography (SPECT)/CT and intratumoral microdistribution analysis indicated TAM-specific localization of the IRD-αCD206 probe in 4T1 tumors after several rounds of sorafenib treatment. Upon light irradiation, IRD-αCD206 suppressed the growth of sorafenib-resistant tumors. In vivo CT imaging and ex vivo histological analysis confirmed the inhibition of lung metastasis in mice by IRD-αCD206 PIT. These results demonstrate the utility of the IRD-αCD206 probe for TAM-targeted diagnostic imaging and treatment of tumors that are resistant to conventional therapeutics.

1. Introduction

Traditional cancer treatments such as radio- and chemotherapy are associated with serious side effects and drug resistance [1]. Although there are many drugs that maximize treatment efficacy while minimizing toxicity, local tumor recurrences and distant metastasis are common, and may eventually lead to drug resistance and treatment failure [2,3].

Sorafenib (BAY 43-9006, Nexavar) is a small molecule tyrosine kinase inhibitor that is approved for the treatment of metastatic renal cell carcinoma and advanced hepatocellular carcinoma [4]. It has also been investigated for the treatment of lung, breast, and other cancers [5,6]. Several clinical studies have found that the patient response rate to this drug is quite low, with cancers becoming sorafenib-resistant after several rounds of therapy [7,8]. Therefore, novel treatments for tumors, especially those that are drug-resistant, are urgently needed.

During cancer development and treatment, tumors are infiltrated by myeloid cells, such as macrophages (tumor-associated macrophages; TAMs), which are recruited in their monocyte precursor form from the peripheral blood [9]. TAM stimulates tumor progression by facilitating angiogenesis, invasion, and metastasis, and suppressing antitumor immunity [10,11]. TAM levels are correlated with poor prognosis in various human cancers and are a major factor in the development of resistance to chemo- or radiotherapy, as well as in tumor recurrence [12,13]. As such,

* Corresponding author.
E-mail address: liuzf@bjmu.edu.cn (Z. Liu).

http://dx.doi.org/10.1016/j.biomaterials.2016.01.027
0142-9612/

characterization of macrophage infiltration in tumors may be used to predict patient outcome and evaluate responses to therapy [14].

TAMs are typically designated as "alternatively activated" non-inflammatory M2-type macrophages, in contrast to the "classically activated" inflammatory "M1" type [15]. TAMs can serve as therapeutic targets or markers for imaging in the evaluation of tumor progression [16]. M2 macrophages specifically express CD206, also known as macrophage mannose receptor [17–19]. CD206-targeted single-photon emission computer tomography (SPECT) or optical imaging can potentially be used as a means of noninvasively visualizing the TAM infiltration into tumors in vivo [20,21].

Antibody- and phthalocyanine dye-based photodynamic therapy (PDT), also known as photoimmunotherapy (PIT) [22], uses the near-infrared phthalocyanine dye IRDye700 as a photosensitizer in conjunction with an antibody that serves as a delivery vehicle for tumor-specific near-infrared fluorescence (NIRF) imaging. Upon light irradiation, PIT selectively destroys malignant cells targeted by antibodies while sparing normal adjacent tissue. The efficacy of PIT has been demonstrated in several tumor models [23–26].

In this study, we synthesized a CD206-targeted PIT probe by conjugating a monoclonal anti-CD206 antibody with IRDye700 and evaluated its effectiveness in vitro and in vivo. We investigated whether the PIT probe could be used to noninvasively visualize and image TAM recruitment to tumors as well as treat tumors that are resistant to sorafenib therapy. Our findings provide information that can be useful for predicting therapeutic response and evaluating drug resistance.

2. Materials and methods

2.1. Cell culture and animal model

The 4T1 murine breast cancer and RAW264.7 murine macrophage cell lines were purchased from American Type Culture Collection. Cells were cultured in RPMI-1640 medium supplemented with 10% (v/v) fetal bovine serum at 37 °C under a humidified atmosphere containing 5% CO_2.

All animal procedures were performed in accordance with the Guidelines of Peking University Animal Care and Use Committee. The 4T1 tumor-bearing mouse model was established by subcutaneous injection of 1×10^6 cells into the right hind legs of female BALB/c mice (5 weeks of age; Department of Laboratory Animal Science, Peking University). The tumor growth was measured using a caliper, and the tumor volume was calculated using the formula: volume = length × width^2/2.

2.2. Sorafenib treatment

The 4T1 tumor-bearing mice with a tumor size of 100–150 mm^3 were selected for in vivo sorafenib treatment studies. A sorafenib dose of 20–50 mg/kg/day has been used in other studies [27–29]. Therefore, 4T1 mice were segregated into four groups (n = 18 per group), and were administered with 0 (vehicle control), 20, 40, or 60 mg sorafenib/kg/day (in 1:1 propylene glycol/water) for 6 days (days 0–5) by gavage. Tumor size and body weight were measured every other day. On day 6, three mice from each group were sacrificed, and their tumors were harvested. After cutting on a freezing microtome, tumor tissues were stained with an anti-CD206 antibody (clone C068C2, IgG2a; BioLegend, San Diego, CA) for 1 h at room temperature and then visualized with dye-conjugated secondary antibody under a Leica TCS-NT confocal microscope (Wetzler, Heidelberg, Germany). Meanwhile, a total of 10 mice from control and 60 mg/kg/day treatment groups (n = 5 per group) were sacrificed and their tumors were digested to obtain single-cell suspensions for flow cytometry analysis.

In separate experiments, 4T1 tumor-bearing BALB/c mice were administered 0 (vehicle control) or 60 mg sorafenib/kg/day (in 1:1 propylene glycol/water) for 6 days (days 0–5) by gavage. These mice were used for in vivo fluorescence and SPECT/CT imaging and in vivo PIT studies.

2.3. Flow cytometry analysis

Harvested tumors were minced into fragments, digested with 10 U/mL collagenase I, 400 U/mL collagenase IV, and 30 U/mL DNase (in phosphate buffered saline; PBS) for 1 h at 37 °C, and then passed through a 70-μm cell strainer. Single-cell suspensions were stained with phycoerythrin (PE)-conjugated rat anti-mouse F4/80 and fluorescein isothiocyanate (FITC)-conjugated rat anti-mouse CD206 antibodies (Sungene, Tianjin, China). Cells were sorted with an LSR-II flow cytometer (Becton Dickinson, Germany).

2.4. Synthesis and in vitro characterization of the anti-CD206 probe

The CD206-targeting probe was generated using a previously described method [30]. Briefly, anti-CD206 antibody (clone C068C2, IgG2a; BioLegend, San Diego, CA) was mixed with IRDye700-N-hydroxysuccinimide (NHS) (LI-COR, Inc. Lincoln, NE) in sodium bicarbonate buffer (pH 8.3) at a 1: 7 mol ratio. After a 12 h incubation at 4 °C, IRDye700-conjugated antibody (IRD-αCD206) was purified using a PD-10 desalting column (GE Healthcare, Piscataway, NJ) using PBS as the mobile phage. The degree of labeling (dye/protein ratio) for IRD-αCD206 was calculated to be approximately 4.1 based on UV measurements. The purity of IRD-αCD206 was determined by sodium dodecyl sulfate polyacrylamide gel electrophoresis (SDS-PAGE) and subsequent NIRF imaging with an IVIS optical imaging system (Xenogen, Alameda, CA). An isotype-matched control probe (IRD-IgG) was synthesized by conjugating rat IgG (IgG2a; BioLegend, San Diego, CA) with IRDye700-NHS using the same protocol.

The immunoreactivity of IRD-αCD206 was evaluated relative to that of the parent antibody (αCD206) with a cell binding assay. Briefly, αCD206 was radiolabeled with Na^{125}I to generate the radiotracer ^{125}I-αCD206 using a previously described protocol [31]. The radiochemical purity of ^{125}I-αCD206 after preparation was >98%. CD206-positive [21] RAW264.7 cells were incubated with ^{125}I-αCD206 in the presence of increasing concentrations of IRD-αCD206 and αCD206 in 96-well filter plates. After incubating for 2 h at 4 °C, the plates were washed using PBS, and the PVDF filters were collected and measured in a γ-counter. Data were fitted with nonlinear regression using GraphPad Prism 5.0 (GraphPad Software, San Diego, CA) (n = 4).

Singlet oxygen of IRD-αCD206 was measured using a singlet oxygen sensor green (SOSG) assay. Briefly, 1.0 μM SOSG (Invitrogen, Carlsbad, CA) was added to IRDye700 (1.0 μM) or IRD-αCD206 (1.0 μM IRDye700 equivalent concentration) solution, followed by irradiation with a 690-nm laser (Shanghai Laser & Optics Century Co., Ltd., Shanghai, China) for various times. SOSG fluorescence was measured with the IVIS optical imaging system (Xenogen, Alameda, CA) at an excitation wavelength of 460 nm and an emission wavelength of 520 nm. In the blocking experiments, the singlet oxygen quencher NaN_3 (50 mM) was added to the solution and singlet oxygen molecules generated by IRD-αCD206 were detected as described above.

2.5. In vivo NIRF imaging

Uptake of IRD-αCD206 by 4T1 tumors in the control or sorafenib-treated BALB/c mice was evaluated by NIRF imaging.

Mice were treated with either the vehicle control or 60 mg sorafenib/kg/day for 6 days (days 0–5). On day 6, each mouse (n = 5 per group) was administered 0.5 nmol IRD-αCD206 by intravenous injection, and in vivo optical imaging was performed at 4, 8, and 24 h postinjection (p.i.). The uptake of IRD-αCD206 by tumor and muscle was determined by normalizing the fluorescence intensity of the tumor by the dose injected [32,33]. After the last scan at 24 h p.i., mice were sacrificed. Tumors and major organs/tissues were dissected, weighed, and ex vivo NIRF imaged. Results are presented as the percent injected dose per gram (%ID/g).

2.6. Small-animal SPECT/CT imaging

4T1 tumor-bearing mice treated with either vehicle control or 60 mg sorafenib/kg/day for 6 days (n = 3 per group) administered 18.5 MBq of ^{125}I-αCD206 by intravenous injection. After anesthetization with 2% isoflurane in oxygen, SPECT and helical CT scans of the mice were performed at 24 h p.i. on a NanoScan SPECT/CT imaging system (Mediso, Budapest, Hungary) [34,35]. The tumor uptake of ^{125}I-αCD206 was quantified using a previously described method [36,37].

2.7. Evaluation of αCD206 microdistribution in sorafenib-treated tumors

After six days (days 0–5) of sorafenib (60 mg/kg/day) treatment, 4T1 tumor-bearing mice were injected intravenously on day 6 with 50 μg FITC-αCD206 (clone C068C2; IgG2a; Sungene, Tianjin, China). At 24 h p.i., tumors were harvested, cut on a freezing microtome, and immunolabeled with an antibody (Abcam, Cambridge, MA) against the M1/M2 macrophage marker F4/80 to determine macrophage localization.

2.8. In vivo PIT

4T1 tumor-bearing mice were treated with vehicle (control group, n = 12) or 60 mg sorafenib/kg/day for 6 days (days 0–5). On day 6, sorafenib-treated mice were randomized into four groups: (1) no treatment (sorafenib group, n = 12); (2) mice injected intravenously with 1 nmol IRD-αCD206 and then irradiated 8, 24, and 48 h p.i. at 70 J/cm^2 with a 690-nm laser (PIT group, n = 12); (3) mice injected with 1 nmol IRD-αCD206 (probe only group, n = 12); (4) mice irradiated 8, 24, and 48 h p.i. at 70 J/cm^2 with a 690-nm laser (light only group, n = 12). Tumor size was measured every other day. On day 10, five mice from each group were sacrificed and their tumors were harvested for histological analysis of Ki67 and terminal deoxynucleotidyl transferase dUTP nick end labeling (TUNEL).

2.9. Assessment of lung metastasis

At the end (day 16) of the in vivo PIT study, lung metastasis was assessed by high-resolution CT imaging and ex vivo examination. Mice were first scanned by CT to determine the position of the chest, and then the lungs were filled with 15% India ink via the upper trachea and fixed in Fekete's solution (100 mL of 70% alcohol, 10 mL of 4% formalin, and 5 mL glacial acetic acid) for 48 h. Metastatic lesions on the black lung surface were counted. Lungs were then fixed with formalin, embedded in paraffin, cut into sections, and stained with hematoxylin and eosin (H&E).

2.10. Immunofluorescence staining

Ki67 and TUNEL fluorescence were determined in order to evaluate the effect of PIT on tumor cell proliferation and apoptosis, respectively. For Ki67 staining, the frozen tumor sections were incubated with rabbit anti-Ki67 (Millipore, Billerica, MA) antibody for 1 h at room temperature and then visualized with dye-conjugated secondary antibodies under a Leica TCS-NT confocal microscope (Wetzler, Heidelberg, Germany). For TUNEL staining, the experiment was conducted by following the manual instruction of In Situ Cell Death Detection kit (Roche, Indianapolis, IN). After staining, 10 random views in the tumor slices were selected for the quantitative analyses. The tumor cell proliferation index and tumor apoptosis were calculated as the percentage of Ki67-positive nuclei and TUNEL-positive nuclei in relation to the total number of nuclei, respectively.

2.11. Validation of PIT specificity

The specificity of IRD-αCD206 PIT for TAMs was evaluated in vitro and in vivo. For in vitro studies, CD206-positive RAW264.7 cells or CD206-negative [21] 4T1 tumor cells were incubated with 10 nM IRD-αCD206 for 1 h at 37 °C. After washing with PBS, cells were irradiated at 0, 5, and 10 J/cm^2 with a 690-nm laser. Propidium iodide (4 mg/mL; Sigma–Aldrich, St. Louis, MO) was added to stain dead cells, which were sorted by flow cytometry.

For in vivo studies, 4T1 tumor-bearing mice were injected intravenously with PBS, 1 nmol of IRD-αCD206 or 1 nmol of IRD-IgG and then irradiated at 8, 24, and 48 h p.i. at 70 J/cm^2 with a 690-nm laser (n = 3 per group). Mice were then sacrificed and their tumors were dissected, cut with a freezing microtome, and immunolabeled with an antibody against F4/80 (to identify macrophages) and evaluated with the TUNEL assay (to identify apoptotic cells) as described above.

2.12. Statistical analysis

Data were analyzed using the GraphPad Prism 5.0 software (GraphPad Software Inc.) and values are presented as mean ± SD. Statistical analysis was done using a 1-way ANOVA for multiple groups and an unpaired Student's t test. P values < 0.05 were considered statistically significant.

3. Results

3.1. Sorafenib treatment has no effect on 4T1 tumor growth

We investigated the therapeutic efficacy of sorafenib in a 4T1 tumor model. After treatment for 6 days, sorafenib administered at doses of 20–60 mg/kg had negligible effects on tumors (Fig. 1A). There was no reduction in body weight at any dose, suggesting that the treatment was not toxic to mice (Fig. 1B).

However, sorafenib increased the number of CD206$^+$F4/80$^+$ M2 macrophages and decreased the number of CD206$^-$F4/80$^+$ M1 macrophages relative to size-matched controls (Fig. 1C, D). These results indicate the repolarization of TAMs and their recruitment to sorafenib-treated tumors. In addition, the M2/M1 ratio was higher for sorafenib-treated as compared to control tumors (65.74 ± 9.17 vs. 45.17 ± 7.48, $P < 0.01$; Fig. 1E).

3.2. Preparation of a TAM-targeted probe

Due to increased M2 macrophage recruitment by sorafenib-treated 4T1 tumors, we hypothesized that CD206 could serve as a biomarker for 4T1 tumors after sorafenib treatment and that a CD206-specific probe would be useful for imaging and therapeutic targeting of sorafenib-treated tumors. We prepared the IRD-αCD206 probe by conjugating an anti-CD206 monoclonal antibody with a photosensitive near-infrared phthalocyanine dye (Fig. 2A).

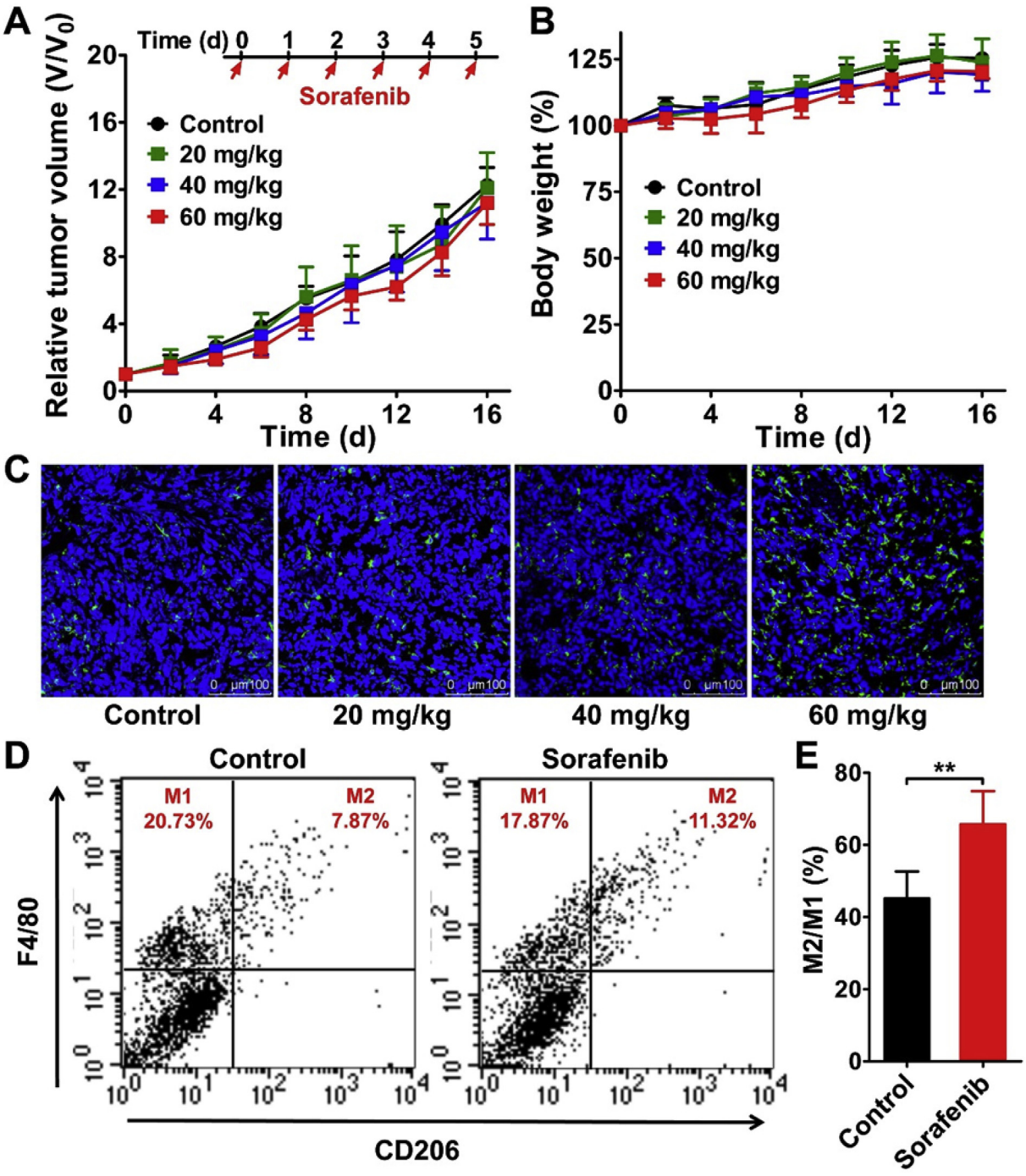

Fig. 1. Sorafenib treatment has no effect on 4T1 tumor growth in vivo but leads to M2 macrophage polarization. (A, B) Tumor growth curves (A) and changes in body weight (B) of 4T1 tumor-bearing BALB/c mice treated daily with vehicle or indicated doses of sorafenib for 6 days. Inset, schedule of sorafenib treatment. (C) Immunofluorescence staining of murine CD206 in 4T1 tumor tissues after vehicle (control) or sorafenib (20, 40, and 60 mg/kg daily for 6 days) treatment. (D, E) Representative dot plots (D) and M2-to-M1 ratios (E) from flow cytometry analyses of F4/80 and CD206 expression by 4T1 tumor cells treated with vehicle or sorafenib sorafenib (60 mg/kg/day for 6 days). **, $P < 0.01$.

The purity of the probe was confirmed by SDS-PAGE and NIRF imaging (Fig. 2B). A competitive cell-binding assay with CD206-positive RAW264.7 cells revealed that IRD-αCD206 (IC_{50} = 11.82 ± 3.44 nM) had CD206-binding affinity that was similar to that of the unmodified antibody (IC_{50} = 8.75 ± 1.97 nM; Fig. 2C).

We measured the singlet oxygen molecules of IRD-αCD206 in PBS solution. As shown in Fig. 2D, E, the singlet oxygen generated after irradiation was increased for both IR700 and IRD-αCD206; these showed near-identical singlet oxygen generation. However, this was significantly inhibited by quenching with NaN_3. These results confirmed the potential utility of IRD-αCD206 for in vitro and in vivo PIT applications.

3.3. *In vivo targeting of tumors by IRD-αCD206*

We investigated whether M2 macrophage recruitment by sorafenib-treated tumors can be noninvasively visualized by in vivo

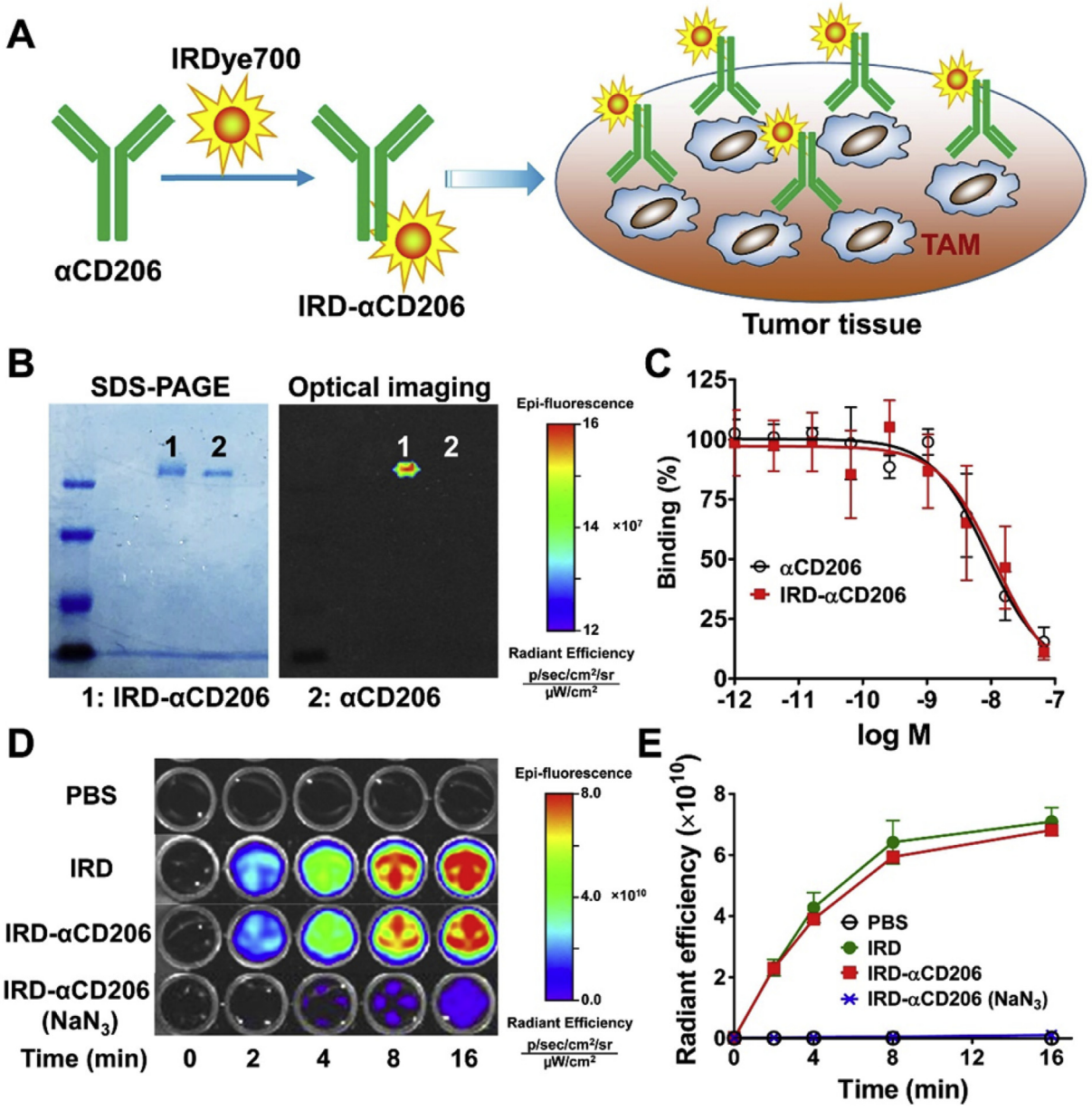

Fig. 2. Synthesis and in vitro characterization of IRD-αCD206. (A) Illustration of the synthesis of IRD-αCD206 for TAM targeting. (B) SDS-PAGE and NIRF imaging of IRD-αCD206 and αCD206. (C) Comparison of the CD206-binding affinities of IRD-αCD206 and αCD206 with the competition binding assay using ^{125}I-αCD206 as a radiotracer in CD206-positive RAW264.7 cells. (D, E) Singlet oxygen generation by IRDye700 and IRD-αCD206 with or without 50 mM NaN_3 quenching after irradiation for indicated periods, as determined by the SOSG assay.

small-animal imaging using the IRD-αCD206 probe. Representative NIRF images of 4T1 tumor-bearing mice with or without sorafenib treatment were examined at different time points after IRD-αCD206 injection (Fig. 3A). Subcutaneous tumors were detected from 4 to 24 h p.i. in both control and sorafenib-treated mice. However, the fluorescence intensity of IRD-αCD206 was significantly higher for sorafenib-treated as compared to control tumors at 4 (5.82 ± 0.38% vs. 4.85 ± 0.15%; $P < 0.01$), 8 (9.20 ± 2.26% vs. 5.98 ± 0.76%; $P < 0.05$) and 24 (9.17 ± 1.97% vs. 5.73 ± 1.49%; $P < 0.05$) h p.i. (Fig. 3B). Tumor-to-muscle IRD-αCD206 ratios were also higher in sorafenib-treated tumors than in controls at 4 (3.13 ± 0.44 vs. 2.08 ± 0.15; $P < 0.01$), 8 (4.98 ± 1.01 vs. 3.36 ± 0.32; $P < 0.01$), and 24 (4.21 ± 0.49 vs. 2.60 ± 0.87; $P < 0.05$) h p.i. (Fig. 3C). These results indicate that more IRD-αCD206 is taken up by sorafenib-treated as compared to untreated tumors. The uptake of IRD-αCD206 in the sorafenib-treated tumors was also significantly higher than that of IRD-IgG at all-time points examined ($P < 0.05$; Fig. S1), demonstrating the CD206-specific targeting of IRD-αCD206.

To validate the in vivo NIRF imaging results, tumors were analyzed by ex vivo NIRF imaging and small-animal SPECT/CT. As shown in Fig. 3D, E, IRD-αCD206 uptake by organs was similar between sorafenib-treated and control mice; however, probe uptake was greater in tumors treated with sorafenib (7.73 ± 1.07%ID/g) as compared to controls (4.71 ± 0.29%ID/g; $P < 0.05$).

Radionuclides are more quantitative than fluorescent dyes, and their in vivo distribution can be accurately and non-invasively quantified by SPECT imaging. We validated the results obtained

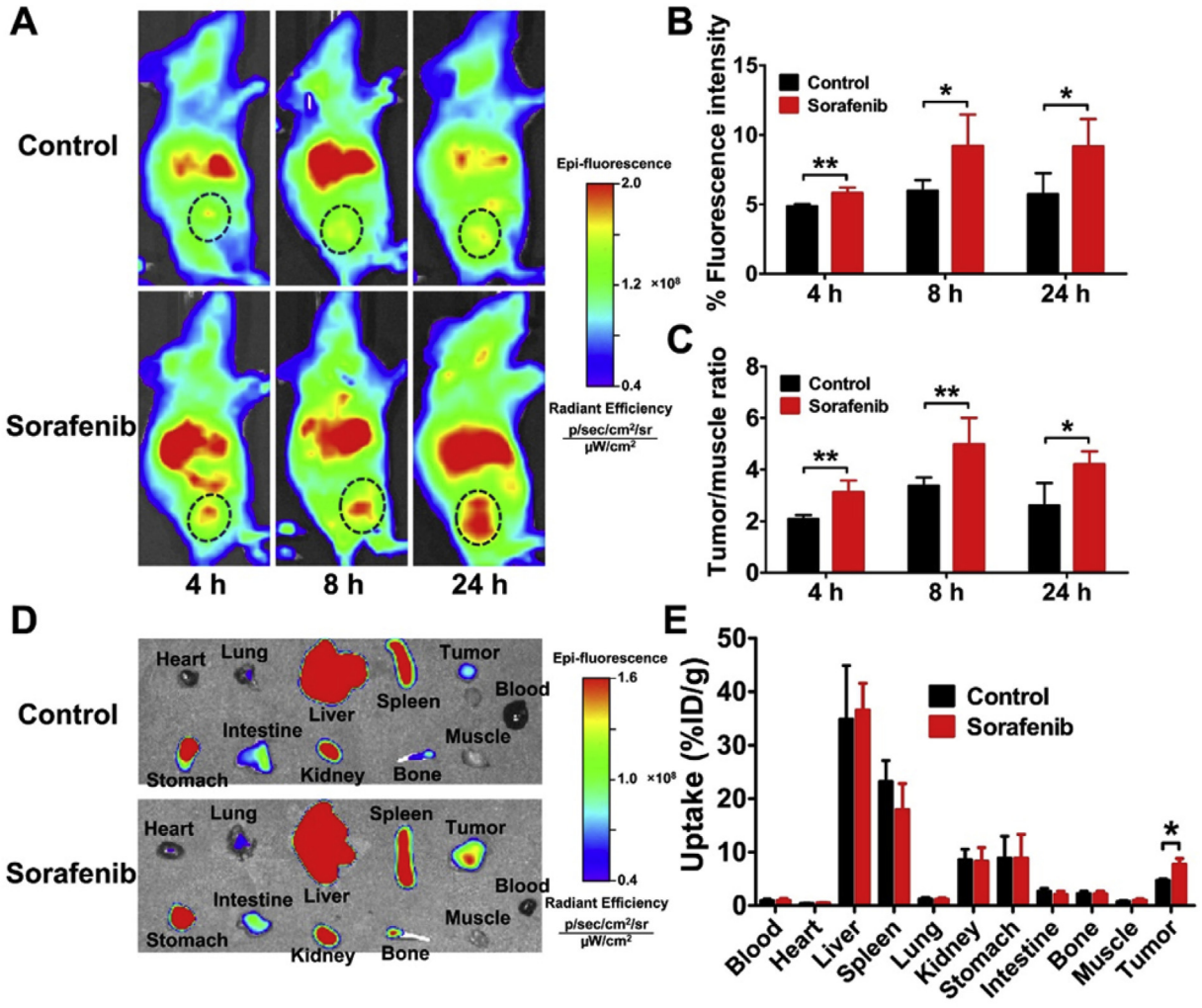

Fig. 3. Uptake of IRD-αCD206 by control or sorafenib (60 mg/kg/day for 6 days)-treated 4T1 tumors. (A) Representative NIRF images at 4, 8, and 24 h after IRD-αCD206 injection. Tumors are indicated with circles. (B, C) Quantitative analysis of uptake (B) and tumor-to-muscle accumulation ratios (C) of IRD-αCD206 in control or sorafenib-treated tumors. (D) Representative images of organs dissected from 4T1 tumor-bearing mice (with or without sorafenib treatment) sacrificed 24 h after intravenous injection of IRD-αCD206. (E) Quantitative analysis of IRD-αCD206 distribution in dissected organs shown in panel D. *, $P < 0.05$; **, $P < 0.01$.

by NIRF imaging of IRD-αCD206 by evaluating its radioactive counterpart ^{125}I-αCD206, which was predominantly taken up by the liver (Fig. 4A) due to hepatic clearance. The probe showed increased accumulation in tumors in sorafenib-treated mice compared to that in the control mice (Fig. 4A). Tomographic imaging revealed a variable distribution of ^{125}I-αCD206 in sorafenib-treated 4T1 tumors (Fig. 4B), reflecting the heterogeneous localization of TAMs. The quantification results confirmed that the uptake of ^{125}I-αCD206 in the sorafenib-treated tumors was significantly higher than that in the control tumors ($P < 0.01$; Fig. 4C).

To confirm the targeting of IRD-αCD206 or ^{125}I-αCD206 to TAMs in sorafenib-treated tumors, we examined tumor tissue from sorafenib-treated 4T1 tumor-bearing mice 24 h after injection of FITC-αCD206 for expression of F4/80 rather than CD206 in order to eliminate the possibility of competitive binding between the anti-CD206 antibody and FITC-αCD206. Note that the anti-CD206 antibody used in FITC-αCD206 was the same clone (C068C2) as that used in IRD-αCD206 or ^{125}I-αCD206. As shown in Fig. 4D, most areas positive for FITC-αCD206 showed F4/80 immunoreactivity, indicating that IRD-αCD206 and ^{125}I-αCD206 were specifically localized in tumors. These results confirm that both probes can be used to image TAMs in vivo.

3.4. IRD-αCD206 PIT prevents growth and metastasis of sorafenib-resistant tumors

IRD-αCD206 PIT of the control tumors without sorafenib treatment showed a remarkable suppression on tumor growth (Fig. S2), which confirms the antitumor effect of PIT. However, the therapy efficacy of IRD-αCD206 PIT is generally limited due to the low expression of CD206 in control tumors. We next investigated whether IRD-αCD206 could be used for in vivo PIT studies of sorafenib-treated tumors (Fig. 5A), which is supposed to express much higher CD206 compared to the control tumors (Fig. 1C, D, E). As shown in Fig. 5B, a time-dependent increase in tumor size was observed in 4T1 tumors treated with vehicle, sorafenib, sorafenib + light, and sorafenib + IRD-αCD206 only. In contrast, a single injection of IRD-αCD206 followed by irradiation at 8, 24, or 48 h p.i. significantly delayed tumor growth relative to the other groups from days 10–16.

We next carried out Ki67 immunolabeling and the TUNEL assay to assess tumor cell proliferation and apoptosis, respectively. As shown in Fig. 5C, the proliferation index was decreased whereas the

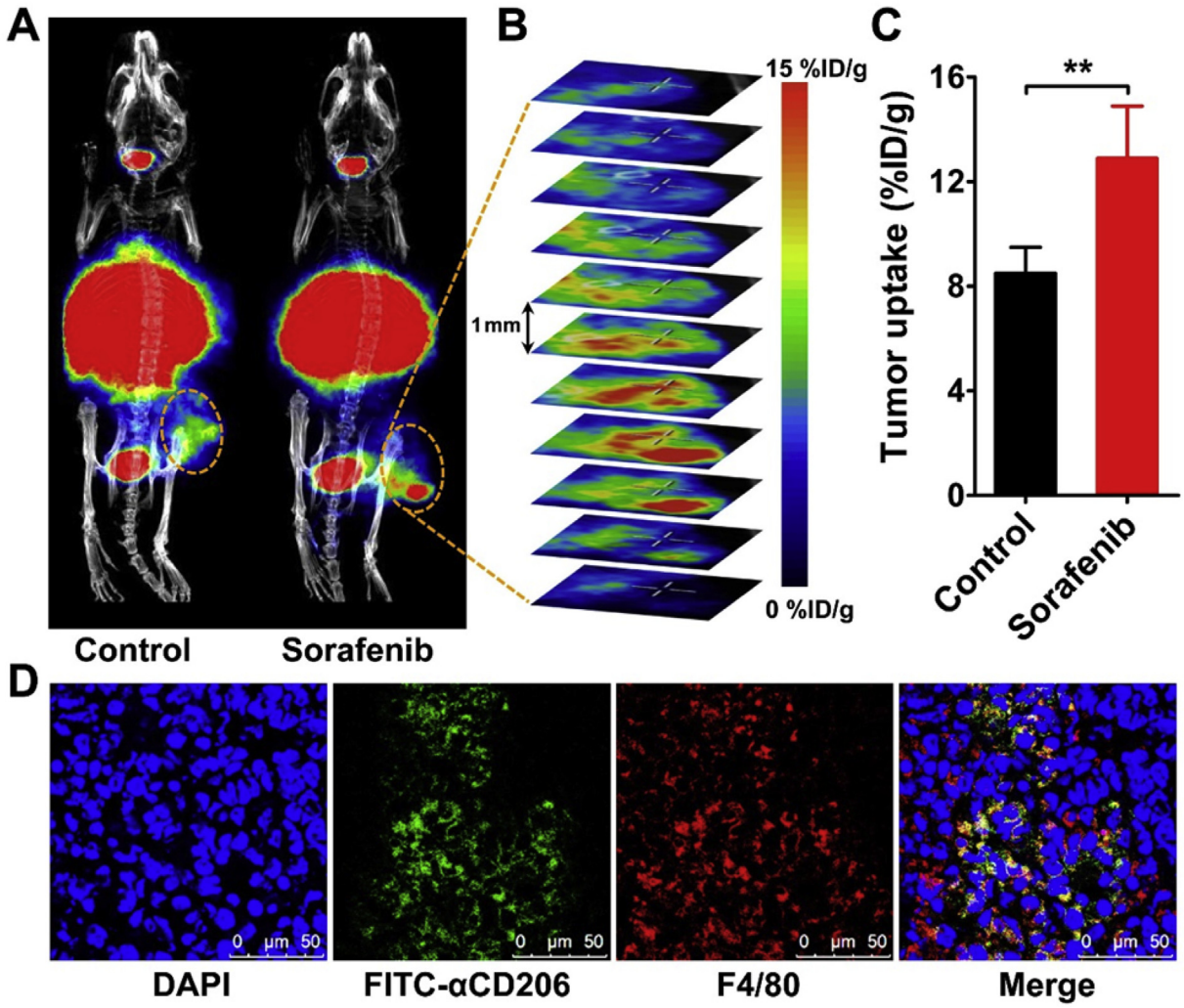

Fig. 4. Macrophage-specific localization of CD206-specific probes in sorafenib-treated 4T1 tumors. (A) Representative small-animal SPECT/CT imaging of ^{125}I-αCD206 24 h post-injection in control or sorafenib (60 mg/kg/day for 6 days)-treated 4T1 tumor-bearing BALB/c mice. Tumors are indicated with circles. (B) Representative 1-mm-thick transaxial slices though a 4T1 syngeneic tumor. (C) Comparison of the quantified uptake of ^{125}I-αCD206 in the control and sorafenib-treated tumors. (D) Distribution of FITC-αCD206 in sorafenib-treated 4T1 tumor tissues harvested from mice 24 h p.i. Green, FITC-αCD206; red, rhodamine corresponding to F4/80; blue, DAPI-stained nuclei. **, P < 0.01. (For interpretation of the references to color in this figure legend, the reader is referred to the web version of this article.)

apoptosis index was increased in the sorafenib + IRD-αCD206 PIT as compared to control groups ($P < 0.001$; Fig. 5D, E), demonstrating the efficacy of IRD-αCD206 PIT for treating sorafenib-resistant 4T1 tumors.

Subcutaneous injection of 4T1 tumor cells in mice results in metastasis to the lungs [21]. We therefore assessed whether IRD-αCD206 PIT can inhibit metastasis of sorafenib-resistant tumors by CT imaging. In control, sorafenib, sorafenib + light only, and sorafenib + IRD-αCD206 only groups, evident metastatic lesions were detected in the lungs; these were negligible in mice in the sorafenib + IRD-αCD206 PIT group (Fig. 6A). These findings were confirmed upon gross examination of lung lesions and by staining lung tissue sections with H&E (Fig. 6B, C). Mice in the sorafenib + IRD-αCD206 PIT group had fewer tumors than those in the control, sorafenib, sorafenib + light only, and sorafenib + IRD-αCD206 only groups ($P < 0.05$; Fig. 6D). These results suggest that TAM-specific PIT can inhibit tumor metastasis to the lungs.

3.5. IRD-αCD206 PIT targets TAMs in sorafenib-resistant tumors

Although IRD-αCD206 PIT prevented lung metastasis of sorafenib-treated 4T1 tumors, the inhibitory effect on subcutaneous tumors was limited; that is, the treatment did not completely prevent tumor growth (Fig. 5B). We hypothesized that one reason for the low efficacy is that target cells (i.e., M2 macrophages) constitute a very small population within the tumors, and photoactivation of IRD-αCD206 is targeted to CD206-positive areas. We therefore compared the cell-ablating capacity of the probe in CD206-positive and -negative cells. Radiation dose-dependent toxicity was observed in CD206-positive RAW264.7 cells (Fig. 7A). However, there was no apoptosis observed in CD206-negative 4T1 cells after irradiation (Fig. 7A).

Tumor-bearing mice were then subjected to IRD-αCD206 PIT, and apoptotic areas of tumor tissues were examined. As shown in Fig. 7B, C, a significantly greater number ($P < 0.01$) of apoptotic cells were detected in IRD-αCD206 PIT as compared to control and IRD-IgG PIT-treated tumors. Importantly, most apoptotic (TUNEL-positive) nuclei in IRD-αCD206 PIT-treated tumors were associated with macrophages showing F4/80 expression at the cell surface. It should be noted that apoptotic tumor cells that are engulfed in macrophages may also be stained by TUNEL and then colocalized with F4/80. However, an almost undetectable cell (both tumor cells

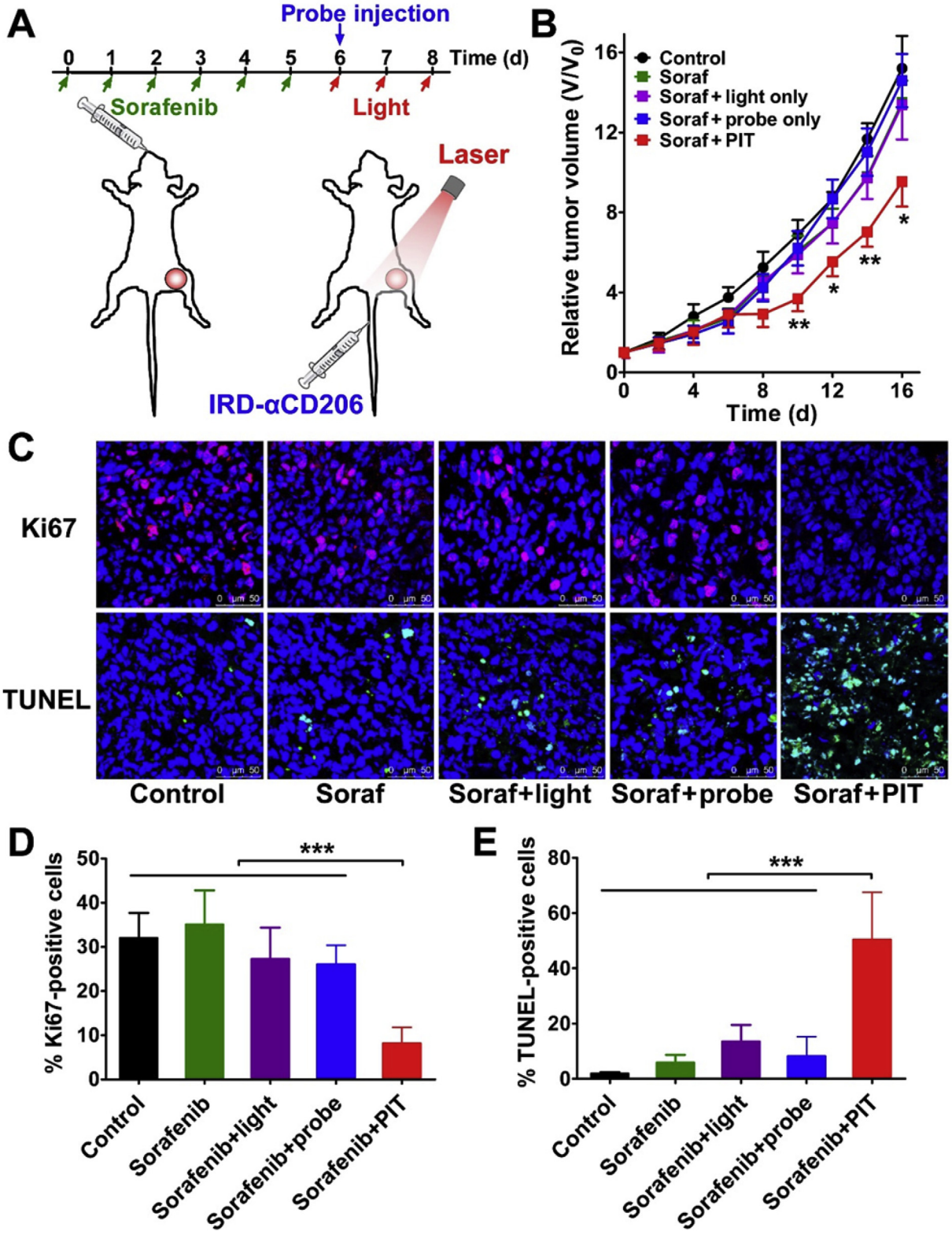

Fig. 5. IRD-αCD206 PIT inhibits the growth of sorafenib (60 mg/kg/day for 6 days)-treated 4T1 tumors in BALB/c mice. (A) Schematic illustration of the PIT protocol in mice. (B) Growth curves of control or sorafenib-treated 4T1 tumors after treatment with light only, IRD-αCD206 (probe) only, or IRD-αCD206 PIT. (C) Histological analysis of proliferating and apoptotic cells in control or sorafenib-treated 4T1 tumor tissue after indicated treatments, as determined by Ki67 immunolabeling and the TUNEL assay, respectively. (D, E) Quantitative analysis of Ki67- (D) and TUNEL- (E) positive cells shown in panel C. *, $P < 0.05$; **, $P < 0.01$; ***, $P < 0.001$.

and macrophages) apoptosis was observed in the control tumor that was not treated with IRD-αCD206 PIT (Fig. 7B, C). Taken together, these data demonstrate that IRD-αCD206 PIT can specifically destroy macrophages in the tumor.

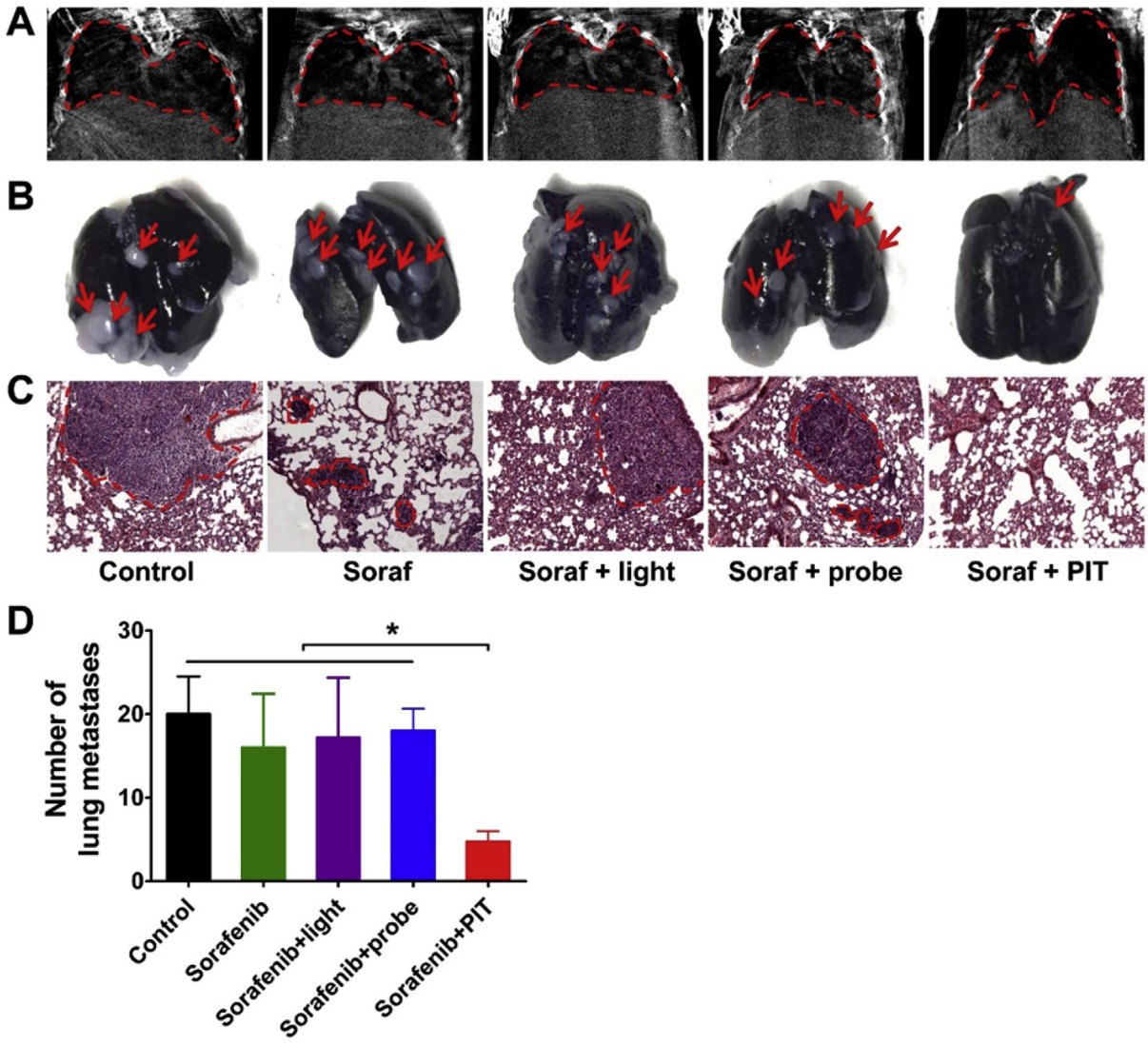

Fig. 6. IRD-αCD206 PIT inhibits lung metastasis of sorafenib (60 mg/kg/day for 6 days)-treated 4T1 tumors in BALB/c mice. (A–C) Representative images from CT scanning (A) and of India ink-filled lungs (B) and H&E-stained lung sections (C) from 4T1 tumor-bearing mice (on day 16) after indicated treatments. Lungs in the CT images and tumor metastases in the H&E-stained lung slices are indicated by dashed circles. Tumor metastases in the India ink-filled lungs are indicated by arrows. (D) Quantitative analysis of lesions in lungs shown in panel B. *, $P < 0.05$.

4. Discussion

In this study we synthesized a probe (IRD-αCD206) targeting sorafenib-resistant tumors and investigated whether it can be used to visualize TAM recruitment and for PIT. We found that TAM recruitment to tumors treated with sorafenib can be detected by IRD-αCD206 NIRF imaging, and that IRD-αCD206 PIT inhibited subcutaneous 4T1 tumor growth and lung metastasis.

We used a 4T1 syngeneic tumor mouse model for in vivo sorafenib treatment. By measuring tumor growth after 6 days of sorafenib treatment, no statistical difference between the tumor sizes with or without sorafenib treatment was observed. In recent studies, Farsaci, et al. [38] observed that 7 days of sorafenib treatment had limited effect on the growth of 4T1 tumors, and only a long-term treatment could lead to the tumor responses to sorafenib. Hammond et al. [39] also demonstrated that sorafenib treatment did not prolong the survival of 4T1 tumor-bearing mice compared to the vehicle control group. These results suggest that 4T1 tumors are resistant to sorafenib treatment.

It is thought that tumor hypoxia following sorafenib treatment plays an essential role in the development of resistance to the drug [7,40,41]. We found that sorafenib had no effect on tumor growth after 6 days of treatment, but increased hypoxia relative to control tumors (Fig. S3), which can lead to the recruitment and activation of various myeloid cells including TAMs [42]. Several studies have demonstrated the recruitment of macrophages after anti-angiogenic therapy or chemotherapy [2,43]. Our study focuses on M2-type macrophage, which is one of the key factors for tumor progression and therapy resistance. The observed increase in M2 macrophage infiltration and CD206 expression in 4T1 tumors treated with sorafenib suggested that CD206 could serve as a marker for TAM infiltration of tumors as well as a target for PIT. In vivo NIRF imaging revealed the accumulation of TAMs in tumors after sorafenib treatment. Given the limitations of planar optical imaging for deep tissue imaging and quantification of fluorescence intensity, we synthesized a radiolabeled analog of IRD-αCD206, namely ^{125}I-αCD206, and evaluated its distribution by small-animal SPECT/CT imaging. The results were in accordance with the optical

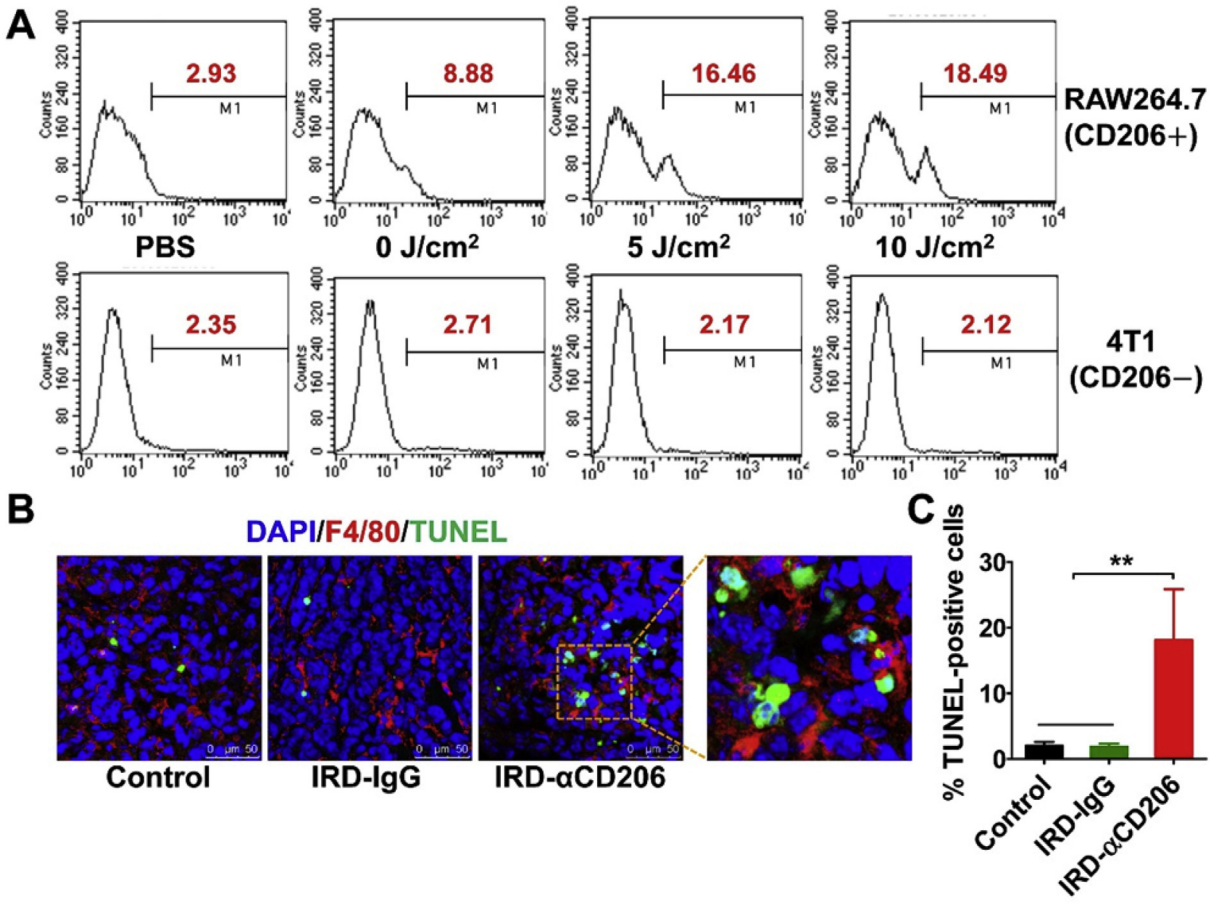

Fig. 7. Macrophage-specific cytotoxicity of IRD-αCD206 PIT in vitro and in vivo. (A) Flow cytometry analysis of dead CD206-positive RAW264.7 or CD206-negative 4T1 cells treated with PBS or IRD-αCD206 PIT (0, 5, and 10 J/cm^2). (B) TUNEL and F4/80 immunolabeling for identification of apoptotic cells and macrophages, respectively, in 4T1 tumor tissues harvested from mice treated with PBS, IRD-IgG or IRD-αCD206 (irradiated at 8, 24, and 48 h p.i. at 70 J/cm^2 for all groups). (C) Quantitative analysis TUNEL-positive cells shown in panel B. **, $P < 0.01$.

imaging data, and demonstrated the localization of ^{125}I-αCD206 in 4T1 tumors. We also confirmed that FITC-αCD206 specifically labeled TAMs. FITC-αCD206 showed only partial overlap with the F4/80 (marker of both M1 and M2 macrophages [44]) signal, which is likely due to the fact that FITC-αCD206 is specific to M2 and not M1 macrophages.

Metastasis is one of the major causes of mortality in cancer patients; evidence suggests that TAMs promote distant tumor metastasis [11,44]. By in vivo CT and ex vivo examination, we observed that the metastasis of subcutaneously inoculated 4T1 tumor cells to the lungs was significantly blocked by depletion of TAMs by IRD-αCD206 PIT. These results demonstrated the anti-metastatic effect of TAM-targeted PIT. Despite robust anti-metastatic effect, the efficacy of IRD-αCD206 PIT in subcutaneous 4T1 tumors treated with sorafenib was sub-optimal, as tumor growth was not entirely eliminated (Fig. 5B). There are two possible reasons for these results. Firstly, IRD-αCD206 targeted TAMs, which represent a small subset of cells in 4T1 tumors, resulting in low uptake of the probe by the tumor, which in turn reduces the effects of PIT; that is, irradiation eliminated only TAMs and not tumor cells. Secondly, like PDT, the effectiveness of PIT depends on the photosensitizer, light, and oxygen [45]; therefore, the hypoxic tumor microenvironment (Fig. S3) of sorafenib-treated 4T1 tumors may reduce the effectiveness of PIT due to a lack of oxygen.

After sorafenib treatment and subsequent CD206-targeted PIT, it did not cause an evident tumor sensitivity to the second rounds of sorafenib treatment (Fig. S4). These results suggest that IRD-αCD206 PIT has limited effect on the reversal of 4T1 tumor resistance to sorafenib. Chen et al. [7] demonstrated that one of the mechanisms underlying sorafenib resistance is the increased tumor hypoxia after sorafenib treatment. Increased hypoxia results in the recruitment and activation of multiple myeloid and lymphoid immune suppressor cells, including M2-type macrophages, myeloid-derived suppressor cells, and T-regulatory cells. Therefore, depletion of M2-type macrophages only (as we used in this study by IRD-αCD206 PIT) may not be sufficient to overcome tumor resistance to sorafenib.

Radiotherapy or chemotherapy with drugs other than sorafenib can also lead to the recruitment of TAMs by resistant tumors [2,46,47]. As such, the present findings can be extended to PIT of tumors treated with other therapies. In addition, several recent studies have shown the synergistic effect of sorafenib in combination with immune checkpoint inhibitors for enhanced antitumor efficacy by activating the function of cytotoxic T lymphocytes and boosting host antitumor immunity [7,48]. PDT has also been reported to be effective on immunopotentiation [45]. Therefore, future studies investigating the combination of PIT and immune checkpoint inhibition to overcome tumor resistance to sorafenib therapy is highly desirable.

5. Conclusion

The results of this study demonstrated that several rounds of sorafenib treatment can lead to M2 macrophage polarization in 4T1 tumors. The recruitment of TAMs by tumors was noninvasively visualized by NIRF imaging of the IRD-αCD206 probe. Upon irradiation, IRD-αCD206 PIT inhibited the growth of subcutaneous 4T1 tumors and prevented their metastasis to the lungs. These results suggest that TAM-targeted PIT is a promising strategy for treating tumors that are resistant to conventional drugs.

Acknowledgments

This work was supported, in part, by the "973" program (2013CB733802 and 2011CB707705), the National Natural Science Foundation of China (81471712, 81222019, 81125011, 81371614, and 81420108019), the Beijing Natural Science Foundation (7132131 and 7132123), and the Beijing Nova Program (Z121107002512010).

Appendix A. Supplementary data

Supplementary data related to this article can be found at http://dx.doi.org/10.1016/j.biomaterials.2016.01.027.

References

[1] W.M. Sharman, J.E. van Lier, C.M. Allen, Targeted photodynamic therapy via receptor mediated delivery systems, Adv. Drug Deliv. Rev. 56 (2004) 53–76.
[2] R. Hughes, B.Z. Qian, C. Rowan, M. Muthana, I. Keklikoglou, O.C. Olson, et al., Perivascular M2 macrophages stimulate tumor relapse after chemotherapy, Cancer Res. 75 (2015) 3479–3491.
[3] L.A. Mina, G.W. Sledge Jr., Rethinking the metastatic cascade as a therapeutic target, Nat. Rev. Clin. Oncol. 8 (2011) 325–332.
[4] J.S. Lagas, R.A. van Waterschoot, R.W. Sparidans, E. Wagenaar, J.H. Beijnen, A.H. Schinkel, Breast cancer resistance protein and P-glycoprotein limit sorafenib brain accumulation, Mol. Cancer Ther. 9 (2010) 319–326.
[5] C.H. Takimoto, A. Awada, Safety and anti-tumor activity of sorafenib (Nexavar) in combination with other anti-cancer agents: a review of clinical trials, Cancer Chemother. Pharmacol. 61 (2008) 535–548.
[6] J. Baselga, J.G. Segalla, H. Roche, A. Del Giglio, H. Pinczowski, E.M. Ciruelos, et al., Sorafenib in combination with capecitabine: an oral regimen for patients with HER2-negative locally advanced or metastatic breast cancer, J. Clin. Oncol. 30 (2012) 1484–1491.
[7] Y. Chen, R.R. Ramjiawan, T. Reiberger, M.R. Ng, T. Hato, Y. Huang, et al., CXCR4 inhibition in tumor microenvironment facilitates anti-programmed death receptor-1 immunotherapy in sorafenib-treated hepatocellular carcinoma in mice, Hepatology 61 (2015) 1591–1602.
[8] J.M. Llovet, S. Ricci, V. Mazzaferro, P. Hilgard, E. Gane, J.F. Blanc, et al., Sorafenib in advanced hepatocellular carcinoma, N. Engl. J. Med. 359 (2008) 378–390.
[9] K. Movahedi, D. Laoui, C. Gysemans, M. Baeten, G. Stange, J. Van den Bossche, et al., Different tumor microenvironments contain functionally distinct subsets of macrophages derived from Ly6C(high) monocytes, Cancer Res. 70 (2010) 5728–5739.
[10] B.Z. Qian, J.W. Pollard, Macrophage diversity enhances tumor progression and metastasis, Cell 141 (2010) 39–51.
[11] M. De Palma, C.E. Lewis, Macrophage regulation of tumor responses to anticancer therapies, Cancer Cell. 23 (2013) 277–286.
[12] A. Sica, P. Invernizzi, A. Mantovani, Macrophage plasticity and polarization in liver homeostasis and pathology, Hepatology 59 (2014) 2034–2042.
[13] W. Zhang, X.D. Zhu, H.C. Sun, Y.Q. Xiong, P.Y. Zhuang, H.X. Xu, et al., Depletion of tumor-associated macrophages enhances the effect of sorafenib in metastatic liver cancer models by antimetastatic and antiangiogenic effects, Clin. Cancer Res. 16 (2010) 3420–3430.
[14] M.R. Junttila, F.J. de Sauvage, Influence of tumour micro-environment heterogeneity on therapeutic response, Nature 501 (2013) 346–354.
[15] A. Mantovani, S. Sozzani, M. Locati, P. Allavena, A. Sica, Macrophage polarization: tumor-associated macrophages as a paradigm for polarized M2 mononuclear phagocytes, Trends Immunol. 23 (2002) 549–555.
[16] Y. Luo, H. Zhou, J. Krueger, C. Kaplan, S.H. Lee, C. Dolman, et al., Targeting tumor-associated macrophages as a novel strategy against breast cancer, J. Clin. Invest 116 (2006) 2132–2141.
[17] P. Allavena, M. Chieppa, G. Bianchi, G. Solinas, M. Fabbri, G. Laskarin, et al., Engagement of the mannose receptor by tumoral mucins activates an immune suppressive phenotype in human tumor-associated macrophages, Clin. Dev. Immunol. 2010 (2010) 547179.
[18] K.M. Choi, P.C. Kashyap, N. Dutta, G.J. Stoltz, T. Ordog, T. Shea Donohue, et al., CD206-positive M2 macrophages that express heme oxygenase-1 protect against diabetic gastroparesis in mice, Gastroenterology 138 (2010), 2399–409, 409 e1.
[19] A.R. Reeves, K.L. Spiller, D.O. Freytes, G. Vunjak-Novakovic, D.L. Kaplan, Controlled release of cytokines using silk-biomaterials for macrophage polarization, Biomaterials 73 (2015) 272–283.
[20] K. Movahedi, S. Schoonooghe, D. Laoui, I. Houbracken, W. Waelput, K. Breckpot, et al., Nanobody-based targeting of the macrophage mannose receptor for effective in vivo imaging of tumor-associated macrophages, Cancer Res. 72 (2012) 4165–4177.
[21] X. Sun, D. Gao, L. Gao, C. Zhang, X. Yu, B. Jia, et al., Molecular imaging of tumor-infiltrating macrophages in a preclinical mouse model of breast cancer, Theranostics 5 (2015) 597–608.
[22] M. Mitsunaga, M. Ogawa, N. Kosaka, L.T. Rosenblum, P.L. Choyke, H. Kobayashi, Cancer cell-selective in vivo near infrared photoimmunotherapy targeting specific membrane molecules, Nat. Med. 17 (2011) 1685–1691.
[23] K. Sato, H. Hanaoka, R. Watanabe, T. Nakajima, P.L. Choyke, H. Kobayashi, Near infrared photoimmunotherapy in the treatment of disseminated peritoneal ovarian cancer, Mol. Cancer Ther. 14 (2015) 141–150.
[24] K. Sato, T. Nagaya, P.L. Choyke, H. Kobayashi, Near infrared photoimmunotherapy in the treatment of pleural disseminated NSCLC: preclinical experience, Theranostics 5 (2015) 698–709.
[25] K. Sato, R. Watanabe, H. Hanaoka, T. Harada, T. Nakajima, I. Kim, et al., Photoimmunotherapy: comparative effectiveness of two monoclonal antibodies targeting the epidermal growth factor receptor, Mol. Oncol. 8 (2014) 620–632.
[26] R. Watanabe, H. Hanaoka, K. Sato, T. Nagaya, T. Harada, M. Mitsunaga, et al., Photoimmunotherapy targeting prostate-specific membrane antigen: are antibody fragments as effective as antibodies? J. Nucl. Med. 56 (2015) 140–144.
[27] Z. Zhang, B. Niu, J. Chen, X. He, X. Bao, J. Zhu, et al., The use of lipid-coated nanodiamond to improve bioavailability and efficacy of sorafenib in resisting metastasis of gastric cancer, Biomaterials 35 (2014) 4565–4572.
[28] M.D. Bareford, M.A. Park, A. Yacoub, H.A. Hamed, Y. Tang, N. Cruickshanks, et al., Sorafenib enhances pemetrexed cytotoxicity through an autophagy-dependent mechanism in cancer cells, Cancer Res. 71 (2011) 4955–4967.
[29] E. Martinelli, T. Troiani, F. Morgillo, G. Rodolico, D. Vitagliano, M.P. Morelli, et al., Synergistic antitumor activity of sorafenib in combination with epidermal growth factor receptor inhibitors in colorectal and lung cancer cells, Clin. Cancer Res. 16 (2010) 4990–5001.
[30] D. Gao, L. Gao, C. Zhang, H. Liu, B. Jia, Z. Zhu, et al., A near-infrared phthalocyanine dye-labeled agent for integrin alphavbeta6-targeted theranostics of pancreatic cancer, Biomaterials 53 (2015) 229–238.
[31] Z. Liu, Z. Yu, W. He, S. Ma, L. Sun, F. Wang, In-vitro internalization and in-vivo tumor uptake of anti-EGFR monoclonal antibody LA22 in A549 lung cancer cells and animal model, Cancer Biother Radiopharm. 24 (2009) 15–24.
[32] T. Ma, H. Liu, X. Sun, L. Gao, J. Shi, H. Zhao, et al., Serial in vivo imaging using a fluorescence probe allows identification of tumor early response to cetuximab immunotherapy, Mol. Pharm. 12 (2015) 10–17.
[33] Z. Liu, X. Sun, H. Liu, T. Ma, J. Shi, B. Jia, et al., Early assessment of tumor response to gefitinib treatment by noninvasive optical imaging of tumor vascular endothelial growth factor expression in animal models, J. Nucl. Med. 55 (2014) 818–823.
[34] Z. Liu, H. Liu, T. Ma, X. Sun, J. Shi, B. Jia, et al., Integrin alphavbeta6-targeted SPECT imaging for pancreatic cancer detection, J. Nucl. Med. 55 (2014) 989–994.
[35] L. Gao, H. Liu, X. Sun, D. Gao, C. Zhang, B. Jia, et al., Molecular imaging of post-Src-inhibition tumor signatures for guiding dasatinib combination therapy, J. Nucl. Med. (2015). DOI: jnumed.115.158881.
[36] Z. Liu, T. Ma, H. Liu, Z. Jin, X. Sun, H. Zhao, et al., ^{177}Lu-labeled antibodies for EGFR-targeted SPECT/CT imaging and radioimmunotherapy in a preclinical head and neck carcinoma model, Mol. Pharm. 11 (2014) 800–807.
[37] X. Yu, Y. Wu, H. Liu, L. Gao, X. Sun, C. Zhang, et al., Small-animal SPECT/CT of the progression and recovery of rat liver fibrosis by using an integrin alphavbeta3-targeting radiotracer, Radiology (2015), http://dx.doi.org/10.1148/radiol.2015150090. Epub.
[38] B. Farsaci, R.N. Donahue, M.A. Coplin, I. Grenga, L.M. Lepone, A.A. Molinolo, et al., Immune consequences of decreasing tumor vasculature with anti-angiogenic tyrosine kinase inhibitors in combination with therapeutic vaccines, Cancer Immunol. Res. 2 (2014) 1090–1102.
[39] E. Hammond, R. Brandt, K. Dredge, PG545, a heparan sulfate mimetic, reduces heparanase expression in vivo, blocks spontaneous metastases and enhances overall survival in the 4T1 breast carcinoma model, PLoS One 7 (2012) e52175.
[40] B. Sennino, D.M. McDonald, Controlling escape from angiogenesis inhibitors, Nat. Rev. Cancer 12 (2012) 699–709.
[41] D.Y. Gao, T. Lin Ts, Y.C. Sung, Y.C. Liu, W.H. Chiang, C.C. Chang, et al., CXCR4-targeted lipid-coated PLGA nanoparticles deliver sorafenib and overcome acquired drug resistance in liver cancer, Biomaterials 67 (2015) 194–203.
[42] G.T. Motz, G. Coukos, The parallel lives of angiogenesis and immunosuppression: cancer and other tales, Nat. Rev. Immunol. 11 (2011) 702–711.
[43] X.D. Liu, A. Hoang, L. Zhou, S. Kalra, A. Yetil, M. Sun, et al., Resistance to antiangiogenic therapy is associated with an immunosuppressive tumor microenvironment in metastatic renal cell carcinoma, Cancer Immunol. Res. 3

(2015) 1017–1029.
[44] B. Ruffell, L.M. Coussens, Macrophages and therapeutic resistance in cancer, Cancer Cell. 27 (2015) 462–472.
[45] A.P. Castano, P. Mroz, M.R. Hamblin, Photodynamic therapy and anti-tumour immunity, Nat. Rev. Cancer 6 (2006) 535–545.
[46] T. Shree, O.C. Olson, B.T. Elie, J.C. Kester, A.L. Garfall, K. Simpson, et al., Macrophages and cathepsin proteases blunt chemotherapeutic response in breast cancer, Genes Dev. 25 (2011) 2465–2479.
[47] G.O. Ahn, D. Tseng, C.H. Liao, M.J. Dorie, A. Czechowicz, J.M. Brown, Inhibition of Mac-1 (CD11b/CD18) enhances tumor response to radiation by reducing myeloid cell recruitment, Proc. Natl. Acad. Sci. U. S. A. 107 (2010) 8363–8368.
[48] T. Motoshima, Y. Komohara, H. Horlad, A. Takeuchi, Y. Maeda, K. Tanoue, et al., Sorafenib enhances the antitumor effects of anti-CTLA-4 antibody in a murine cancer model by inhibiting myeloid-derived suppressor cells, Oncol. Rep. 33 (2015) 2947–2953.